Journal of Applied Physics

Stable and hard hafnium borides: A first-principles study

Cite as: J. Appl. Phys. **125**, 205109 (2019); https://doi.org/10.1063/1.5092370
Submitted: 11 February 2019 . Accepted: 03 May 2019 . Published Online: 29 May 2019

Congwei Xie, Qi Zhang, Hayk A. Zakaryan, Hao Wan, Ning Liu, Alexander G. Kvashnin, and Artem R. Oganov

COLLECTIONS

Note: This paper is part of the Special Topic on Ultra-Hard Materials.

This paper was selected as an Editor's Pick

View Online Export Citation CrossMark

ARTICLES YOU MAY BE INTERESTED IN

Axial silicon-germanium nanowire heterojunctions: Structural properties and carrier transport
Journal of Applied Physics **125**, 205107 (2019); https://doi.org/10.1063/1.5091934

Single-layer BiOBr: An effective p-type 2D thermoelectric material
Journal of Applied Physics **125**, 205111 (2019); https://doi.org/10.1063/1.5098826

Simple and accurate model of fracture toughness of solids
Journal of Applied Physics **125**, 065105 (2019); https://doi.org/10.1063/1.5066311

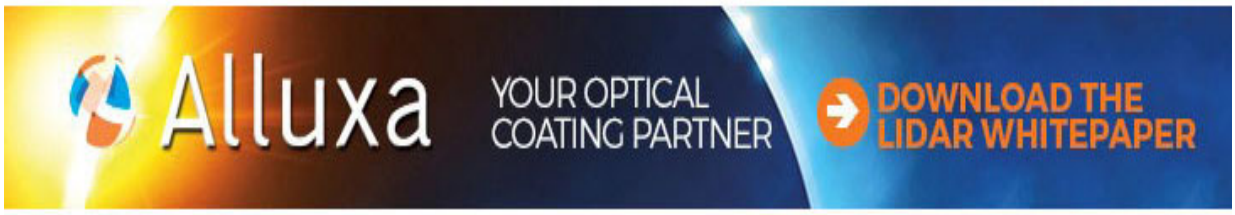

© 2019 Author(s).

Journal of Applied Physics | ARTICLE | scitation.org/journal/jap

Stable and hard hafnium borides: A first-principles study

Cite as: J. Appl. Phys. **125**, 205109 (2019); doi: 10.1063/1.5092370
Submitted: 11 February 2019 · Accepted: 3 May 2019 ·
Published Online: 29 May 2019

View Online Export Citation CrossMark

Congwei Xie,[1,2,3,a)] Qi Zhang,[1,4,a)] Hayk A. Zakaryan,[5] Hao Wan,[6] Ning Liu,[7] Alexander G. Kvashnin,[3,b)] and Artem R. Oganov[1,2,3,b)]

AFFILIATIONS

[1]State Key Laboratory of Solidification Processing, School of Materials Science and Engineering, Northwestern Polytechnical University, Xi'an 710072, China
[2]International Center for Materials Discovery, School of Materials Science and Engineering, Northwestern Polytechnical University, Xi'an 710072, China
[3]Skolkovo Institute of Science and Technology, Skolkovo Innovation Center, 3 Nobel Street, Moscow 121205, Russia
[4]Science and Technology on Thermostructural Composite Materials Laboratory, School of Materials Science and Engineering, Northwestern Polytechnical University, Xi'an 710072, China
[5]Yerevan State University, 1 Alex Manoogian St., 0025 Yerevan, Armenia
[6]Caihong Group Co., Ltd., Xianyang 712021, China
[7]Xi'an Particle Cloud Biotechnology Co., Ltd., Xi'an 710077, China

Note: This paper is part of the Special Topic on Ultra-Hard Materials.
[a)]**Contributions:** C. Xie and Q. Zhang contributed equally to this work.
[b)]**Authors to whom correspondence should be addressed:** A.Kvashnin@skoltech.ru and A.Oganov@skoltech.ru

ABSTRACT

We investigate the stability of hafnium borides at zero pressure via the evolutionary crystal structure prediction and first-principles calculations. Our results indicate that the well-known $P6/mmm$-HfB_2 is the only thermodynamically stable phase at zero temperature and pressure, and two more phases ($Pnma$-HfB and $Fm\bar{3}m$-HfB_{12}) become thermodynamically stable at higher temperatures. We compute the mechanical properties including bulk, shear and Young's moduli, Vickers hardness, and fracture toughness for all stable and metastable hafnium borides (~30 phases) and then study in detail the effect of boron concentration and topology of B-sublattice on their mechanical properties. We show that not only the concentration of boron, but also the topology of the boron sublattice is important for the mechanical properties of hafnium borides. Among the predicted stable and low-energy metastable hafnium borides, the highest possible hardness is exhibited by $P6/mmm$-HfB_2 with graphenelike boron sheets and by phases with 3D boron networks and high B/Hf ratios (e.g., $Pnnm$-HfB_5 and $Fm\bar{3}m$-HfB_{12}).

Published under license by AIP Publishing. https://doi.org/10.1063/1.5092370

I. INTRODUCTION

Transition metal borides (TMBs) are important materials for many practical applications due to their high strength and hardness,[1–3] high melting temperature,[4,5] good corrosion and oxidation resistance,[6,7] electrical conductivity,[8] and other properties. Like most TMBs, they share common features like a facile synthesis at ambient pressure, diverse stoichiometries, and tunable properties changing with the B/TM ratio. Motivated by these features, many studies have been performed to discover/design novel TMBs with superior properties (e.g., potentially superhard CrB_4[9] and WB_5,[10] high strength highly conductive ZrB_{12},[8] etc.).

Among TMBs, hafnium borides are known as ultrahigh-temperature structural ceramics.[11–13] Experimentally, besides the well-known $P6/mmm$-HfB_2, two more Hf_xB_y phases ($Pnma$-HfB[11] and $Fm\bar{3}m$-HfB_{12}[11,14]) have been synthesized at high temperatures. Several experimental and theoretical studies argued that HfB has

Published under license by AIP Publishing.

the $Fm\bar{3}m$ space group.[11,12] However, there are theoretical studies where the correct symmetry was determined as *Pnma*.[15–17] Theoretically, several other Hf_xB_y structures, such as $I4/mcm$-Hf_2B,[12] *Cmcm*-HfB,[18] $P\bar{6}m2$-HfB,[19] $R\bar{3}m$-HfB,[19] *Immm*-Hf_3B_4,[20] $C2/m$-HfB_3,[21] and *Cmcm*-HfB_4,[22,23] have been studied. Although the structures of hafnium borides have been discussed for many decades, a comprehensive study of their thermodynamic stability is still lacking.

The mechanical properties of hafnium borides have been widely investigated.[12,19,21,22,24,25] Hafnium borides with high B contents (HfB_2, HfB_3, HfB_4, and HfB_{12}) were found to have high strength and hardness.[22] HfB_2,[12] HfB_3,[21] and HfB_4[22] were suggested to be potentially superhard materials as indicated by their very high theoretical hardness (more than 40 GPa). We note that boron content is not the only factor that determines the mechanical properties of TMBs; boron motifs (ranging from 0D isolated boron atoms and boron dimers to 1D boron chains and ribbons and to 2D/3D boron frameworks) in TMBs also affect the mechanical properties drastically.[26–28]

In the present study, we use the variable-composition evolutionary crystal structure prediction algorithm USPEX[29–31] to explore the thermodynamically stable and metastable hafnium borides. Diverse stoichiometries (Hf_2B, Hf_3B_2, Hf_7B_6, HfB, Hf_3B_4, Hf_2B_3, HfB_2, HfB_3, HfB_4, HfB_5, HfB_6, and HfB_{12}) and many types of boron configurations (zigzag chain, ribbon, graphenelike sheet, double layer, triple layer, and 3D framework) were found. We have updated the ground-state structures for Hf_2B, Hf_3B_4, and HfB_4 and several newly predicted hafnium borides (Hf_3B_2, Hf_7B_6, Hf_2B_3, HfB_5, and HfB_6). Based on ∼30 stable and low-energy metastable hafnium borides, we defined the correlation between B content, configuration of the B-sublattice, and computed mechanical properties. We show that not only the concentration of boron but also the topology of the boron sublattice has a strong effect on the mechanical properties of hafnium borides.

II. COMPUTATIONAL METHODS

To explore stable and metastable hafnium borides, we performed a variable-composition evolutionary crystal structure prediction for the Hf–B system. The maximum number of atoms in a primitive cell of the generated Hf_xB_y structures was set at 28. During the structure search, the first generation (120 structures) was produced randomly, while the succeeding generations were obtained using heredity (40%), softmutation (20%), and transmutation (20%) operators, and the remaining 20% of each generation was randomly produced.

The VASP code[32,33] was used for structure relaxations and total energy calculations in the framework of the density functional theory.[34] The Perdew–Burke–Ernzerhof generalized gradient approximation (GGA-PBE[35]) was used to treat the exchange-correlation energy, and the projector-augmented wave (PAW) method[36] was employed to describe core–valence interactions with [Xe4f^{14}] and [He] core configurations for Hf and B, respectively. We chose the plane-wave kinetic cut-off energy of 500 eV and uniform k-point meshes for sampling the Brillouin zone with a reciprocal-space resolution of $2\pi \times 0.05$ Å^{-1}.

Stable hafnium borides were identified by the thermodynamic convex hull construction, which compactly presents the thermodynamic information about all possible formation and decomposition reactions. Stable compounds are located on the convex hull, while metastable ones are located above the convex hull at a given temperature and pressure. To construct the thermodynamic convex hull, the enthalpy of formation ΔH_f (normalized per atom) of each generated Hf_xB_y structure was computed in the following way:

$$\Delta H_f(\mathrm{Hf}_x\mathrm{B}_y) = [H(\mathrm{Hf}_x\mathrm{B}_y) - xH(\mathrm{Hf}) - yH(\mathrm{B})]/(x+y), \quad (1)$$

where $H(\mathrm{Hf}_x\mathrm{B}_y)$, $H(\mathrm{Hf})$, and $H(\mathrm{B})$ are the enthalpies of Hf_xB_y structure and ground-state structures of hafnium (*hcp*-Hf, $P6_3/mmc$) and boron (we used α-B, which is energetically degenerate with disordered ground-state β-boron), respectively.

For all stable Hf_xB_y structures and low-energy metastable structures, we have performed the phonon calculations using the finite displacement method as implemented in the PHONOPY code[37] to confirm their dynamical stability. To check the mechanical stability of these Hf_xB_y structures, the single-crystal elastic constants C_{ij} were calculated by the stress–strain approach[38] using the VASP code.[32,33] The elastic constants of a mechanically stable crystal satisfy the Born–Huang criteria.[39] To calculate the phonon dispersion curves and mechanical properties, a denser k-points mesh with a reciprocal-space resolution of $2\pi \times 0.03$ Å^{-1} was used.

By utilizing the computed C_{ij} of predicted Hf_xB_y structures, using the Voigt–Reuss–Hill averaging,[40] we derived their bulk moduli (B), shear moduli (G), Young's moduli (Y), Pugh's ratios ($k = G/B$), and Poisson's ratios (ν). We used the Chen–Niu empirical model[41] to estimate the Vickers hardness H_v of the predicted Hf_xB_y phases,

$$H_v = 2 \cdot (k^2 \cdot G)^{0.585} - 3, \quad (2)$$

where H_v and G are expressed in GPa. The fracture toughness K_{IC} was estimated by the Niu–Niu–Oganov empirical model,[42]

$$K_{IC} = V_0^{1/6} \cdot G \cdot (B/G)^{1/2}, \quad (3)$$

where V_0 is the volume per atom. For several Hf_xB_y structures, we have also computed their ideal tensile (σ, in GPa) and shear (τ, in GPa) strengths which are the maximum stresses reached in the stress–strain curves for a given direction and slip system.

III. RESULTS AND DISCUSSIONS

A. Stability of hafnium borides

1. Zero-temperature stability

Our variable-composition evolutionary crystal structure prediction calculations immediately give the information about stable and metastable hafnium borides at ambient pressure and $T = 0$ K. Figure 1 shows the thermodynamic convex hull of the Hf–B system, and it shows that the well-known $P6/mmm$-HfB_2 is the only thermodynamically stable hafnium boride at ambient pressure and zero temperature. For the other two experimentally reported hafnium borides (*Pnma*-HfB and $Fm\bar{3}m$-HfB_{12}), our prediction shows that they are metastable at zero temperature, in agreement with the previous theoretical studies.[19]

Published under license by AIP Publishing.

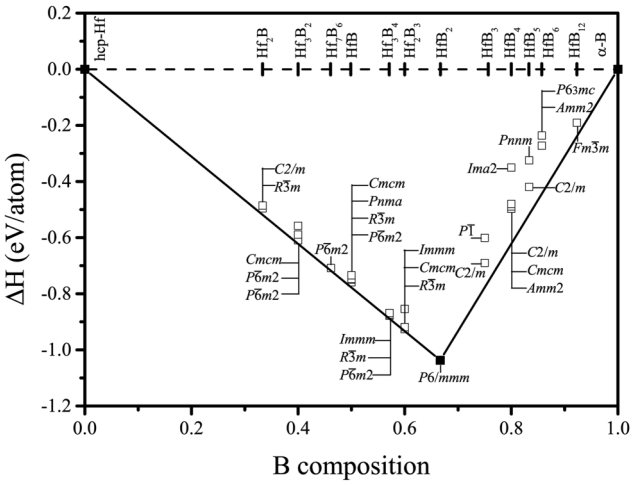

FIG. 1. Thermodynamic convex hull of the Hf–B binary system at 0 K.

Besides recovering these three experimentally reported hafnium borides, we have also predicted many metastable hafnium borides which are close to the thermodynamic convex hull: Hf_2B, Hf_3B_2, Hf_7B_6, HfB, Hf_3B_4, Hf_2B_3, HfB_3, HfB_4, HfB_5, and HfB_6, as shown in Fig. 1. Our predicted lowest-energy structures for HfB ($P\bar{6}m2$) and HfB_3 ($C2/m$) are the same as those reported in the previous studies.[19,21] For Hf_2B, Hf_3B_4, and HfB_4, previous works suggested space groups $I4/mcm$,[12] $Immm$,[20] and $Cmcm$,[22] respectively. Now, $I4/mcm$-Hf_2B is replaced by the more stable $R\bar{3}m$-Hf_2B, $Immm$-Hf_3B_4 by $P\bar{6}m2$-Hf_3B_4, and $Cmcm$-HfB_4 by $Amm2$-HfB_4. Hf_3B_2 ($P\bar{6}m2$), Hf_7B_6 ($P\bar{6}m2$), Hf_2B_3 ($R\bar{3}m$), HfB_5 ($C2/m$), and HfB_6 ($Amm2$) are newly predicted structures. For most of these metastable hafnium borides, besides the lowest-energy structures at zero temperature, we report several other low-energy structures for each composition (see Fig. 1).

Crystal structures of the predicted stable and metastable hafnium borides are listed in Table I and Table SI in the supplementary material. For the known structures, we give both experimental and theoretical values[12,16,18,20–22] for comparison, and one can see a very good agreement.

TABLE I. Computed formation enthalpy ΔH and thermodynamical stability for all the predicted hafnium borides at zero temperature and pressure along with B motifs in their structures.

Phase	Space group	B motif	ΔH (eV/atom)	Instability (eV/atom)
Hf_2B	$R\bar{3}m$	Graphenelike layer	−0.496	0.022
	$C2/m$	Zigzag chain	−0.486	0.033
Hf_3B_2	$P\bar{6}m2$	Graphenelike layer	−0.610	0.013
	$P\bar{6}m2$	Graphenelike layer	−0.589	0.033
	$Cmmm$	Zigzag chain	−0.558	0.064
Hf_7B_6	$P\bar{6}m2$	Graphenelike layer	−0.708	0.009
HfB	$P\bar{6}m2$	Graphenelike layer	−0.759	0.019
	$R\bar{3}m$	Graphenelike layer	−0.749	0.028
	$Pnma$	Zigzag chain	−0.747	0.030
	$Cmcm$	Zigzag chain	−0.734	0.043
Hf_3B_4	$P\bar{6}m2$	Graphenelike layer	−0.878	0.010
	$R\bar{3}m$	Graphenelike layer	−0.874	0.014
	$Immm$	Ribbon	−0.868	0.020
Hf_2B_3	$R\bar{3}m$	Graphenelike layer	−0.926	0.007
	$Cmcm$	Ribbon	−0.919	0.014
	$Immm$	3D framework	−0.854	0.079
HfB_2	$P6/mmm$	Graphenelike layer	−1.037	0
HfB_3	$C2/m$	Graphenelike layer and Bilayer	−0.690	0.087
	$P\bar{1}$	3D framework	−0.600	0.177
HfB_4	$Amm2$	Graphenelike layer and Trilayer	−0.497	0.125
	$Cmcm$	Bilayer	−0.489	0.133
	$C2/m$	Bilayer	−0.480	0.142
	$Ima2$	3D framework	−0.351	0.271
HfB_5	$C2/m$	3D framework	−0.419	0.099
	$Pmmn$	3D framework	−0.324	0.194
HfB_6	$Amm2$	Trilayer	−0.272	0.172
	$P6_3mc$	3D framework	−0.236	0.208
HfB_{12}	$Fm\bar{3}m$	3D framework	−0.191	0.049

Published under license by AIP Publishing.

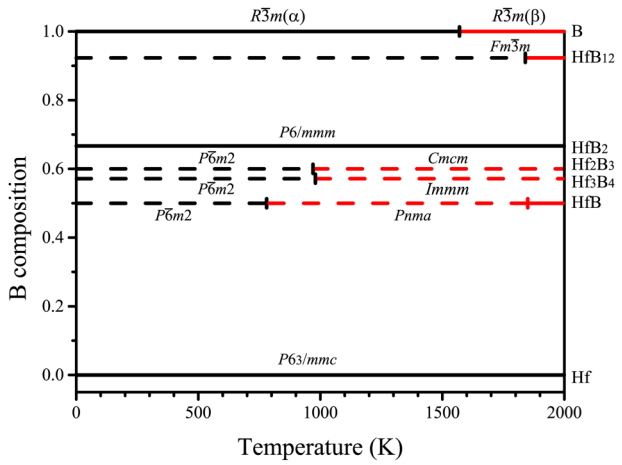

FIG. 2. Temperature-composition phase diagram of the Hf–B binary system calculated by the QHA method from 0 to 2000 K.

To verify the dynamical stability of the predicted stable and metastable hafnium borides, we have calculated their phonon dispersion curves (see Fig. S1 in the supplementary material). There are no imaginary phonon frequencies, which indicates dynamical stability. We computed the elastic constants of all the predicted hafnium borides to check their mechanical stability (see Table SII in the supplementary material). All hafnium borides were found to be mechanically stable because their elastic constants fulfill the Born–Huang criteria.[39]

2. High-temperature stability

Compounds that are metastable at zero temperature may become stable and possible to synthesize as the environmental conditions (e.g., pressure and temperature) change. We have performed a detailed study of the thermodynamic stability of all predicted low-energy Hf_xB_y phases to see whether any phases are stabilized by temperature. We computed Gibbs free energies at zero pressure and temperatures in the range from 0 to 2000 K using the quasiharmonic approximation (QHA).[43] We constructed convex hulls at different temperatures (see Fig. S2 in the supplementary material) and composition-temperature phase diagram (see Fig. 2). We see that *Pnma*-HfB and $Fm\bar{3}m$-HfB_{12}, metastable at zero temperature, become thermodynamically stable at high temperatures, in agreement with the experiment.[11] According to the computed composition-temperature diagram (Fig. 2), *Pnma*-HfB and $Fm\bar{3}m$-HfB_{12} are thermodynamically stable at temperatures above 1850 K and 1840 K, respectively.

Temperature also induces a phase transition in HfB: as shown in Fig. 2, $P\bar{6}m2$-HfB has slightly lower energy than *Pnma*-HfB at low temperatures (T < 780 K); however, at high temperatures (>780 K), *Pnma*-HfB has lower Gibbs free energy than $P\bar{6}m2$-HfB. Similar temperature-induced phase transitions are also predicted for metastable Hf_3B_4 and Hf_2B_3 (see Fig. 2). Clearly, one has to consider not only the lowest-energy structures but also low-energy metastable structures when studying phase stability at nonzero temperatures.

B. B configurations in hafnium borides

Table I lists the phases studied here and provides the types of boron sublattices for them. We found 6 main types of boron sublattices: zigzag chain, ribbon, graphenelike sheet, bilayer, trilayer, and 3D framework in predicted hafnium borides. Crystal structures of hafnium borides with mentioned configuration types are shown in Fig. 3.

Let us consider Hf_xB_y phases with the B/Hf ratio less than or equal to 1. Boron atoms in these structures mainly adopt two types of configurations: 2D graphenelike sheet and 1D zigzag chain. The former configuration is more favorable at ambient pressure and zero temperature, while the latter may become favorable at high temperatures, as suggested by the cases of $P\bar{6}m2$- and *Pnma*-Hf_2B.

At $1 < B/Hf \leq 2$, the graphenelike B-sheet is also adopted by the lowest-energy structures of Hf_3B_4, Hf_2B_3, and HfB_2 ($P\bar{6}m2$-Hf_3B_4, $R\bar{3}m$-Hf_2B_3, and $P6/mmm$-HfB_2) at zero temperature. Besides the 2D graphenelike B-sheet, we also found 1D B-ribbons in metastable *Immm*-Hf_3B_4 and *Cmcm*-Hf_2B_3, and a 3D B-framework in metastable *Immm*-Hf_2B_3. This is the first time that B atoms were found in 3D connectivity in a boride with such a low B content.

For borides with B/Hf > 2, boron atoms form either 2D multiple-layer sublattices or 3D frameworks. In $C2/m$-HfB_3, *Cmcm*-HfB_4, and $C2/m$-HfB_4, boron bilayers were found, while structures of *Amm*2-HfB_4 and *Amm*2-HfB_6 contain boron trilayers. In other hafnium borides ($P\bar{1}$-HfB_3, *Ima*2-HfB_4, $C2/m$-HfB_5, *Pnnm*-HfB_5, $P6_3mc$-HfB_6, and $Fm\bar{3}m$-HfB_{12}), boron atoms form 3D networks.

C. Mechanical properties of hafnium borides

The mechanical properties including elastic moduli (bulk B, shear G, and Young's modulus Y), Pugh's ratio (G/B), Poisson's ratio (ν), Vickers hardness (H_v), and fracture toughness (K_{IC}) of all predicted stable and metastable hafnium borides are summarized in Table II. Whenever possible, we also list the previously reported theoretical or experimental values,[12,16,18,20–22,44,45] and one can see a good agreement with the previous studies.[12,16,18,20–22,44,45]

For a well-known high-temperature structural material HfB2 ($P6/mmm$), our calculation confirms the superior mechanical properties (B: 262 GPa, G: 248 GPa, E: 565 GPa, H_v: 44.1 GPa). Previous theoretical studies[12] suggest that the elastic moduli and hardness of $P6/mmm$-HfB_2 are higher than those of other hafnium borides. From Table II we can find that there are several newly predicted hafnium borides (HfB_3, HfB_4, HfB_5, and HfB_6) with elastic moduli and hardness comparable to HfB_2, suggesting that boron-rich hafnium borides are promising structural materials. These boron-rich phases have lower density compared to HfB_2 (e.g., 7.15 g/cm^3 for *Amm*2-HfB_6 vs 11.13 g/cm^3 for $P6/mmm$-HfB_2) and higher fracture toughness (e.g., 3.57 MPa m$^{1/2}$ for *Amm*2-HfB_6 vs 3.03 MPa m$^{1/2}$ for $P6/mmm$-HfB_2).

Besides the boron content, we can also find that the topology (more specifically, dimensionality) of the boron sublattice has a strong effect on the mechanical properties. Hf_xB_y phases with the same boron content show wide variation in the elastic moduli and Vickers hardness (see Table II and Fig. 4). Interestingly, the mechanical properties of boron-rich Hf_xB_y phases with $y/x = 1.5$–12 and with 3D boron networks do not show a dependence on boron

Published under license by AIP Publishing.

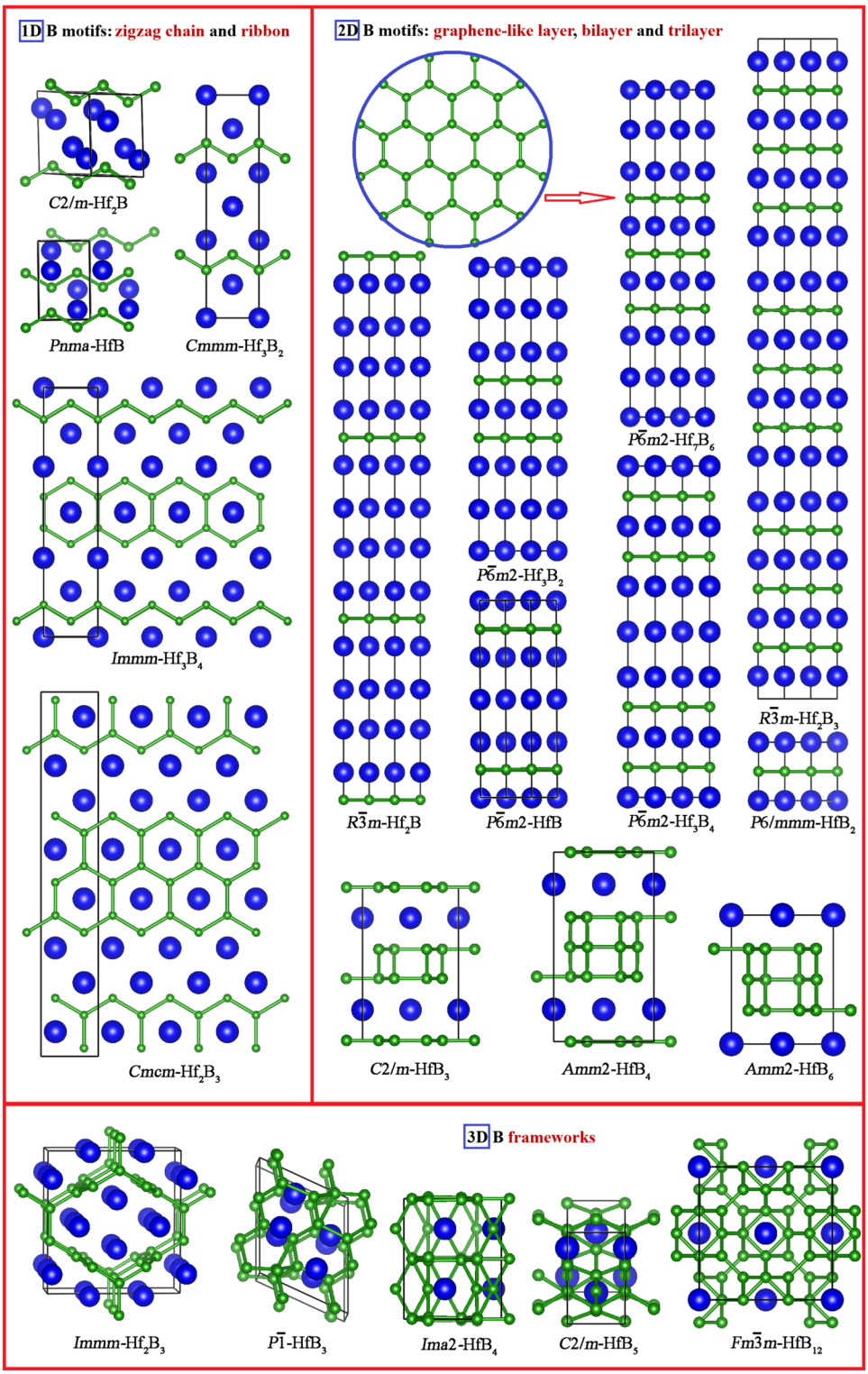

FIG. 3. Crystal structures of several hafnium borides: Hf atoms are shown as blue spheres, B atoms as green spheres.

Published under license by AIP Publishing.

TABLE II. Calculated mechanical properties including elastic bulk modulus B (GPa), shear modulus G (GPa), Young's modulus E (GPa), Poisson's ratio v, Pugh's ratio G/B, Vickers hardness H_v (GPa), and fracture toughness K_{IC} (MPa m$^{1/2}$) of hafnium borides.

Phase	Space group	B	G	E	υ	G/B	H_v	K_{IC}
Hf_2B	$R\bar{3}m$	146	83	208	0.262	0.565	10.6	1.8
	$C2/m$	151	94	235	0.241	0.626	13.6	1.9
Hf_3B_2	$P\bar{6}m2$	161	102	253	0.239	0.632	14.5	2.0
	$P\bar{6}m2$	160	99	246	0.244	0.618	13.8	2.0
	$Cmmm$	161	113	275	0.214	0.706	18.2	2.1
Hf_7B_6	$P\bar{6}m2$	175	114	281	0.233	0.651	16.3	2.2
HfB	$P\bar{6}m2$	184	127	310	0.219	0.691	19.1	2.4
	$R\bar{3}m$	179	115	283	0.236	0.642	16.1	2.2
	$Pnma$	206	166	392	0.184	0.809	28.1	2.8
	$Cmcm$	204	164	388	0.182	0.807	27.7	2.8
	Ref. 16 ($Pnma$)	231	178	424	0.194	0.769	26.8	
	Ref. 16 ($Cmcm$)	208	174	408	0.172	0.840	26.3	
	Ref. 18 ($Cmcm$)	208	168			0.806		
Hf_3B_4	$P\bar{6}m2$	208	154	372	0.202	0.743	24.0	2.7
	$R\bar{3}m$	209	151	366	0.208	0.725	22.9	2.7
	$Immm$	223	193	449	0.165	0.864	33.6	3.1
	Ref. 20 ($Immm$)	227	196	457	0.165		33.9	
Hf_2B_3	$R\bar{3}m$	221	166	399	0.199	0.754	25.6	2.9
	$Cmcm$	232	206	477	0.158	0.887	36.2	3.3
	$Immm$	226	182	430	0.183	0.805	29.5	3.0
HfB_2	$P6/mmm$	262	248	565	0.141	0.945	44.1	3.7
	Ref. 12 ($P6/mmm$)	260	235	542	0.153	0.901	40.3	
	Ref. 22 ($P6/mmm$)	253	246	558	0.133	0.971	45.5	
	Ref. 44 ($P6/mmm$)						31.5	
	Ref. 45 ($P6/mmm$)						19.8	3.3
HfB_3	$C2/m$	255	225	521	0.160	0.881	37.9	3.5
	$P\bar{1}$	256	228	527	0.156	0.892	38.9	3.5
	Ref. 21 ($C2/m$)	248	229	525	0.147	0.920	40.8	
HfB_4	$Amm2$	256	246	558	0.136	0.9611	44.8	3.6
	$Cmcm$	249	239	543	0.137	0.958	43.8	3.5
	$C2/m$	250	227	523	0.152	0.906	39.6	3.4
	$Ima2$	245	213	496	0.162	0.871	36.2	3.3
	Ref. 22 ($Cmcm$)	243	240	542	0.128	0.987	45.7	
HfB_5	$C2/m$	238	223	510	0.143	0.938	40.9	3.3
	$Pmmn$	228	197	459	0.164	0.865	34.2	3.1
HfB_6	$Amm2$	252	253	568	0.124	1.004	48.1	3.6
	$P6_3mc$	250	180	436	0.209	0.721	25.5	3.0
HfB_{12}	$Fm\bar{3}m$	238	182	435	0.195	0.767	27.8	2.9
	Ref. 12 ($Fm\bar{3}m$)	237	204	476	0.166	0.862	34.7	

content (see Table II and green squares in Fig. 4). A general rule is that structures with strong and isotropic three-dimensional covalent boron networks, which withstand large tensile/shear strain, should have high mechanical strength and hardness.[46]

D. Are hafnium borides intrinsically superhard materials?

According to the Chen–Niu empirical model, a number of Hf_xB_y phases studied here exhibit Vickers hardness H_v exceeding 40 GPa (a threshold for defining superhard materials). However, perfect models of materials hardness do not exist, and we resort to a double-check. We consider a material unquestionably superhard if its estimated Vickers hardness and computed ideal tensile and shear strengths are both above 40 GPa—we note that most of the known intrinsically superhard materials possess very high ideal tensile strength σ and shear strength τ together with high Vickers hardness; see the cases of diamond [H_v: 96 GPa,[41] $|\min(\sigma, \tau)|$: 92.8 GPa[47]], c-BN [H_v: 66 GPa,[41] $|\min(\sigma, \tau)|$: 65 GPa[47]], B_6O [H_v: > 40 GPa,[48] $|\min(\sigma, \tau)|$: 38 GPa[46]], etc. For this reason, we have computed the ideal tensile and shear strengths for 12 predicted Hf_xB_y phases (including all stable structures and several metastable structures with computed

Published under license by AIP Publishing.

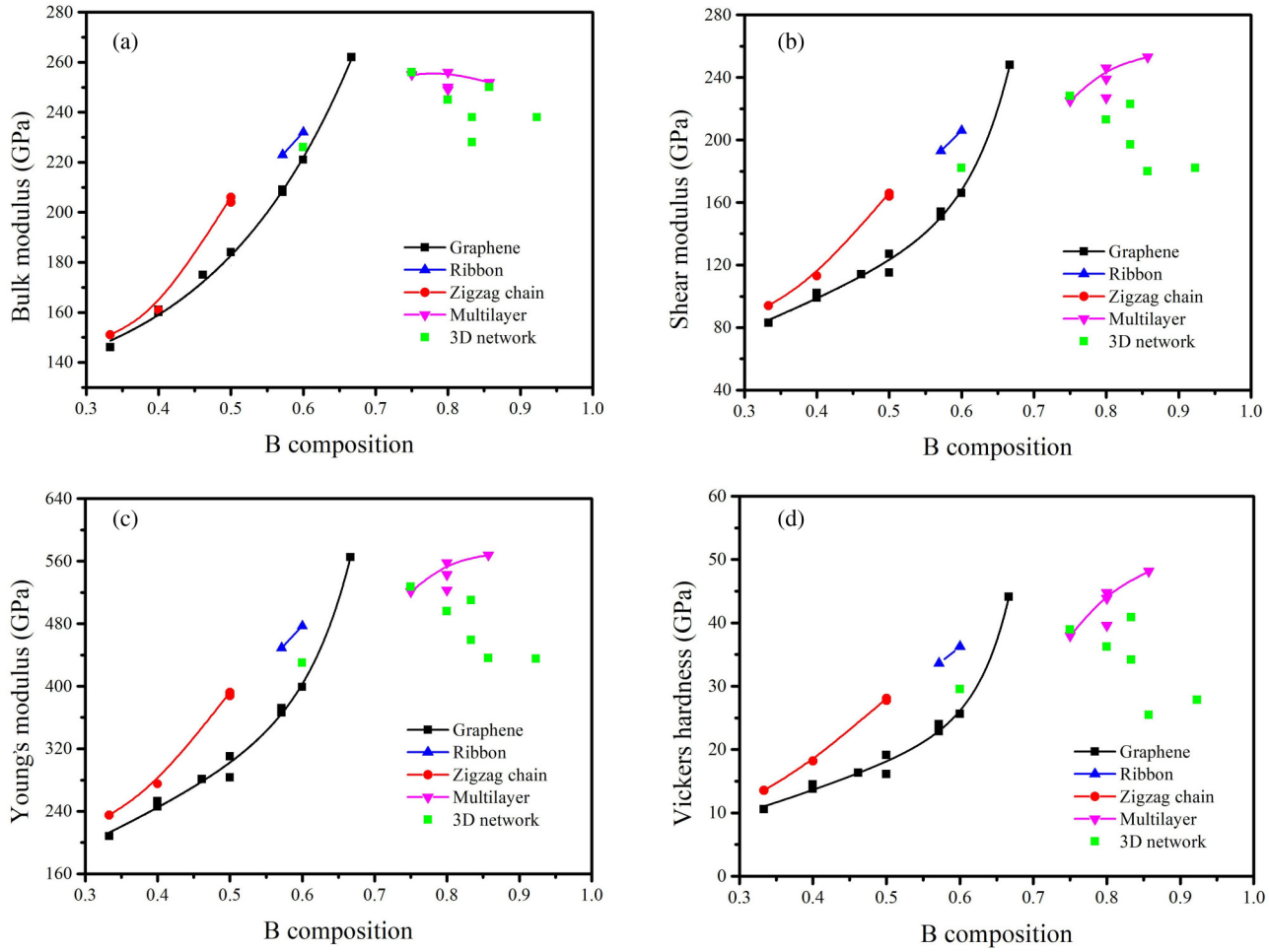

FIG. 4. Mechanical properties including bulk modulus (*B*), shear modulus (*G*) and Young's modulus vs B content and B configuration. (a) Bulk modulus, (b) shear modulus, (c) Young's modulus, and (d) Vickers hardness.

H_v higher than 30 GPa), as listed in Table III; stress–strain curves are shown in Fig. S3 in the supplementary material. For the known *P*6/*mmm*-HfB_2, we have also listed the previously reported values[49] for comparison. Our calculations agree well with the previous work.

According to Table III, *P*6/*mmm*-HfB_2 and $Fm\bar{3}m$-HfB_{12} are the only two phases with ideal strengths higher than 30 GPa, which confirms that they are very hard and possibly superhard materials. The experimentally determined hardness for *P*6/*mmm*-HfB_2 is much lower than the predicted value, in the range from 20 to 32 GPa.[44,45] For $Fm\bar{3}m$-HfB_{12}, there is no experimentally measured hardness. Recently, Akopov *et al.*[14] synthesized five $Fm\bar{3}m$-$Y_xHf_{1-x}B_{12}$ ($x = 0$, 0.05, 0.25, 0.5, and 0.75) samples. The experimentally measured Vickers hardness for all those samples at high load (4.9 N) is in the range of 28–32 GPa.[14] Based on their data, the derived Vickers hardness for pure $Fm\bar{3}m$-HfB_{12} should be around 30 GPa, which is close to the ideal strength, but below 40 GPa (the threshold for defining superhard materials).

Both the predicted hardness of *Pnnm*-HfB_5 (34 GPa) and its ideal strength (25 GPa) suggest that *Pnnm*-HfB_5 should be a hard material. Except for *P*6/*mmm*-HfB_2, $Fm\bar{3}m$-HfB_{12}, and *Pnnm*-HfB_5, the calculated ideal strengths for other phases are lower than their predicted hardness, and none of these phases has an ideal strength higher than 21 GPa.

The diverse values of ideal strength and hardness of hafnium borides can be explained by the chemical bonding in their structures. The well-known *P*6/*mmm*-HfB_2 has high ideal strength and hardness because of strong Hf–B bonds linking the two-dimensional covalently bonded graphenelike boron sheets and making the material withstand large tensile/shear strains. We remind that Hf–B bonds in Hf_xB_y compounds should be partially covalent because of the significant hybridization between Hf-5*d* and B-2*p* orbitals and large ELF values between Hf atoms and their neighboring B atoms.[21,22] For Hf_xB_y phases with low B contents (e.g., $P\bar{6}m2$-HfB), the hardness is low because of the presence of

Published under license by AIP Publishing.

TABLE III. Calculated ideal tensile σ (GPa) and shear τ (GPa) strength of hafnium borides.

		Tensile		Shear	
Phase	Space group	Direction	σ_{min}	Slip system	τ_{min}
HfB	$P\bar{6}m2$	[001]	21.5	(001)[1–10]	3.7
	Pnma	[001]	14.0	(101)[−101]	10.4
Hf_3B_4	*Imam*	[001]	18.8	(011)[01–1]	25.1
Hf_2B_3	*Cmcm*	[010]	20.7	(011)[0–11]	26.4
	Immm	[110]	21.8	(010)[100]	16.8
HfB_2	*P6/mmm*	[1–10]	34.9	(110)[1–10]	36.2
	Ref. 49	[210]	37.3	(100)[010]	33.3
HfB_4	*Amm2*	[111]	27.3	(100)[011]	15.2
	Cmcm	[111]	17.0	(001)[110]	9.5
	Ima2	[101]	28.1	(101)[10–1]	18.1
HfB_5	*Pmmn*	[101]	31.7	(100)[011]	24.7
HfB_6	*Amm2*	[111]	29.0	(100)[011]	15.0
HfB_{12}	$Fm\bar{3}m$	[110]	49.9	(111)[−1–12]	32.1

relatively soft Hf layers in their structures (see Fig. 3). Several boron-rich Hf_xB_y phases such as *Pnnm*-HfB_5 and $Fm\bar{3}m$-HfB_{12} possess high ideal strength and hardness. This is attributed to strong three-dimensional boron networks and the absence of pure metallic Hf–Hf layers in their structures; see Fig. 3 and Fig. S3 in the supplementary material. We note that the formation of a strong 3D covalent boron network would be a good way to enhance the hardness of TMBs. However, this is not the only way because of the diverse features of 3D boron networks. For instance, we have computed the ideal strength and hardness for a newly predicted HfB_6 phase ($P6_3mc$) with the 3D B-network and found that it has much lower hardness and ideal strength than *Pnnm*-HfB_5 and $Fm\bar{3}m$-HfB_{12}, as listed in Table III. For boron-rich Hf_xB_y phases with multilayer boron "sandwiches," we found that none of them have high mechanical properties. This happens because such Hf_xB_y phases undergo structural phase transformations under small tensile/shear strains. Figure 5 shows the case of a phase transition in HfB_4.

Among all the studied hafnium borides, three (HfB_2, HfB_5, and HfB_{12}) are hard and potentially superhard materials. To clearly achieve superhardness, effective intrinsic and extrinsic hardening effects such as the formation of solid solution,[14] going to nanoscale,[50] and grain hardening[51] would be needed.

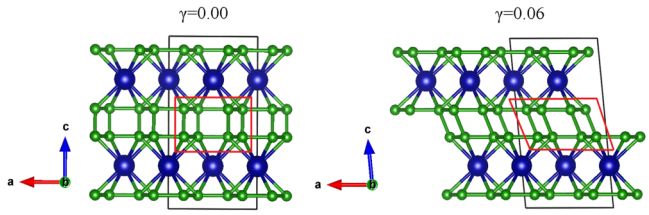

FIG. 5. Phase transition of HfB_4 under shear strain γ in the (001)[110] slip system: *Cmcm* phase ($\gamma = 0.00$) to *C2/c* phase ($\gamma = 0.06$).

IV. CONCLUSIONS

Using the evolutionary crystal structure prediction method USPEX combined with first-principles calculation, we investigated the stability of hafnium borides at zero pressure. We confirmed that the well-known *P6/mmm*-HfB_2 is the only thermodynamically stable phase at zero temperature and pressure. With an increase in temperature, two more phases (*Pnma*-HfB and $Fm\bar{3}m$-HfB_{12}) become thermodynamically stable at 1850 K and 1840 K, respectively. Besides these three stable Hf_xB_y phases, we also discovered many metastable phases with rich stoichiometries (Hf_2B, Hf_3B_2, Hf_7B_6, HfB, Hf_3B_4, Hf_2B_3, HfB_3, HfB_4, HfB_5, and HfB_6) and diverse boron configurations (zigzag chain, ribbon, graphenelike sheet, double layer, triple layer, and 3D framework). We defined the correlation between boron content, boron sublattice type, and mechanical properties by considering both stable and metastable hafnium borides (~30 phases). For boron-poor Hf_xB_y phases ($y/x < 2$), an increase in the boron content leads to the hardening of the material. Moreover, the structures with 1D zigzag boron chain and ribbon configurations have higher mechanical characteristics than their counterparts with 2D graphenelike boron layers. Among all stable and low-energy metastable predicted Hf_xB_y phases, the highest possible hardness is exhibited by *P6/mmm*-HfB_2 with graphenelike B-sheet and boron-rich structures with 3D boron networks, namely *Pnnm*-HfB_5 and $Fm\bar{3}m$-HfB_{12}. There are also several boron-rich phases such as HfB_3, HfB_4, and HfB_6 with 2D boron multilayered sublattice that are comparable to *P6/mmm*-HfB_2 by their elastic moduli, but their hardness is much lower because they undergo phase transitions under small strains.

SUPPLEMENTARY MATERIAL

The supplementary material includes data on the crystal structure of the predicted stable and metastable hafnium borides together with data on the elastic constants, phonon dispersion curves, thermodynamic convex hulls at finite temperatures, and stress–strain curves.

ACKNOWLEDGMENTS

We acknowledge the Natural Science Foundation of China (Grant Nos. 51672218 and 51632007), the Foreign Talents Introduction and Academic Exchange Program of China (Grant No. B08040), and the Russian Science Foundation (Grant No. 17-73-20038). We acknowledge the High Performance Computing Center of NWPU for the allocation of computing time on their machines.

REFERENCES

[1] R. B. Kaner, J. J. Gilman, and S. H. Tolbert, Science **308**, 1268 (2005).
[2] X. Zhang, J. Qin, X. Sun, Y. Xue, M. Ma, and R. Liu, Phys. Chem. Chem. Phys. **15**, 20894 (2013).
[3] A. G. Kvashnin, A. R. Oganov, A. I. Samtsevich, and Z. Allahyari, J. Phys. Chem. Lett. **8**, 755 (2017).
[4] W. G. Fahrenholtz, G. E. Hilmas, I. G. Talmy, and J. A. Zaykoski, J. Am. Ceram. Soc. **90**, 1347 (2007).
[5] R. A. Andrievski, Russ. Chem. Rev. **74**, 1061 (2005).
[6] C. Martini, G. Palombarini, and M. Carbucicchio, J. Mater. Sci. **39**, 933 (2004).
[7] M. M. Opeka, I. G. Talmy, E. J. Wuchina, J. A. Zaykoski, and S. J. Causey, J. Eur. Ceram. Soc. **19**, 2405 (1999).

Published under license by AIP Publishing.

[8]T. Ma, H. Li, X. Zheng, S. Wang, X. Wang, H. Zhao, S. Han, J. Liu, R. Zhang, P. Zhu, Y. Long, J. Cheng, Y. Ma, Y. Zhao, C. Jin, and X. Yu, Adv. Mater. **29**, 1604003 (2017).
[9]H. Niu, J. Wang, X. Q. Chen, D. Li, Y. Li, P. Lazar, R. Podloucky, and A. N. Kolmogorov, Phys. Rev. B **85**, 144116 (2012).
[10]A. Kvashnin, H. A. Zakaryan, C. Zhao, Y. Duan, Y. A. Kvashnina, C. Xie, H. Dong, and A. R. Oganov, J. Phys. Chem. Lett. **9**, 3470 (2018).
[11]P. Rogl and P. Potter, Calphad **12**, 207 (1988).
[12]Y. Pan, H. Huang, X. Wang, and Y. Lin, Comput. Mater. Sci. **109**, 1 (2015).
[13]G. Akopov, M. T. Yeung, and R. B. Kaner, Adv. Mater. **29**, 1604506 (2017).
[14]G. Akopov, M. T. Yeung, C. L. Turner, R. L. Li, and R. B. Kaner, Inorg. Chem. **55**, 5051 (2016).
[15]F. Failamani, K. Göschl, G. Reisinger, C. A. Nunes, G. C. Coelho, A. J. S. Machado, L. E. Correa, J. C. P. dos Santos, G. Giester, and P. Rogl, J. Phase Equilib. Diffus. **36**, 620 (2015).
[16]B. Huang, Y.-H. Duan, W.-C. Hu, Y. Sun, and S. Chen, Ceram. Int. **41**, 6831 (2015).
[17]H. Bittermann and P. Rogl, J. Phase Equilib. **18**, 24 (1997).
[18]X. Xu, K. Fu, L. Li, Z. Lu, X. Zhang, Y. Fan, J. Lin, G. Liu, H. Luo, and C. Tang, Phys. B **419**, 105 (2013).
[19]X. T. Wei, Q. F. Zeng, Q. Zhang, and Q. H. Feng, Chin. J. Inorg. Chem. **34**, 3 (2018).
[20]N. Miao, B. Sa, J. Zhou, and Z. Sun, Comput. Mater. Sci. **50**, 1559 (2011).
[21]L.-H. Huang, Y.-R. Zhao, G.-T. Zhang, M.-G. Zhang, P.-Y. Li, and Y.-F. Hu, Mol. Phys. **117**, 547 (2018).
[22]G. Zhang, R. Gao, Y. Zhao, T. Bai, and Y. Hu, J. Alloys Compd. **723**, 802 (2017).
[23]J. Chang, X. Zhou, K. Liu, and N. Ge, R. Soc. Open Sci. **5**, 180701 (2018).
[24]T. Cheng, W. Li, and W. Y. Ching, J. Am. Ceram. Soc. **98**, 190 (2015).
[25]S. N. Dub, A. A. Goncharov, S. S. Ponomarev, V. B. Filippov, G. N. Tolmacheva, and A. V. Agulov, J. Superhard Mater. **33**, 151 (2011).
[26]Q. Li, D. Zhou, W. Zheng, Y. Ma, and C. Chen, Phys. Rev. Lett. **115**, 185502 (2015).
[27]Y. Pan, Y. H. Lin, J. M. Guo, and M. Wen, RSC Adv. **4**, 47377 (2014).
[28]Y. Pan and Y. Lin, J. Phys. Chem. C **119**, 23175 (2015).
[29]A. R. Oganov and C. W. Glass, J. Chem. Phys. **124**, 201 (2006).
[30]A. R. Oganov, A. O. Lyakhov, and M. Valle, Acc. Chem. Res. **44**, 227 (2011).
[31]A. O. Lyakhov, A. R. Oganov, H. T. Stokes, and Q. Zhu, Comput. Phys. Commun. **184**, 1172 (2013).
[32]G. Kresse and J. Hafner, Phys. Rev. B **49**, 14251 (1994).
[33]G. Kresse and J. Furthmüller, Phys. Rev. B **54**, 11169 (1996).
[34]W. Kohn and L. J. Sham, Phys. Rev. **140**, A1133 (1965).
[35]J. P. Perdew, K. Burke, and M. Ernzerhof, Phys. Rev. Lett. **77**, 3865 (1996).
[36]P. E. Blöchl, Phys. Rev. B **50**, 17953 (1994).
[37]A. Togo, F. Oba, and I. Tanaka, Phys. Rev. B **78**, 134106 (2008).
[38]Y. Le Page and P. Saxe, Phys. Rev. B **65**, 104104 (2002).
[39]O. Beckstein, J. E. Klepeis, G. L. W. Hart, and O. Pankratov, Phys. Rev. B **63**, 134112 (2001).
[40]R. Hill, Proc. Phys. Soc. **65**, 349 (2002).
[41]X. Q. Chen, H. Niu, D. Li, and Y. Li, Intermetallics **19**, 1275 (2011).
[42]H. Niu, S. Niu, and A. R. Oganov, J. Appl. Phys. **125**, 065105 (2018).
[43]D. C. Wallace, *Thermodynamics of Crystals* (Courier Corporation, 1972).
[44]L. Bsenko and T. Lundström, J. Less Common Met. **34**, 273 (1974).
[45]E. Zapata-Solvas, D. D. Jayaseelan, H. T. Lin, P. Brown, and W. E. Lee, J. Eur. Ceram. Soc. **33**, 1373 (2013).
[46]R. F. Zhang, Z. J. Lin, Y. S. Zhao, and S. Veprek, Phys. Rev. B **83**, 092101 (2011).
[47]Y. Zhang, H. Sun, and C. Chen, Phys. Rev. Lett. **93**, 195504 (2004).
[48]D. He, Y. Zhao, L. Daemen, J. Qian, T. D. Shen, and T. W. Zerda, Appl. Phys. Lett. **81**, 643 (2002).
[49]X. Zhang, X. Luo, J. Li, P. Hu, and J. Han, Scr. Mater. **62**, 625 (2010).
[50]S. Vepřek, A. S. Argon, and R. F. Zhang, Philos. Mag. **90**, 4101 (2010).
[51]S. Vepřek and S. Reiprich, Thin Solid Films **268**, 64 (1995).

Published under license by AIP Publishing.